Irregular Wind Power Plant Dynamics Induced by Power Factor Command Truncation

Bikal Pudasaini
Dominion Energy, Inc.
Glen Allen, VA, USA
bikal.pudasaini@dominionenergy.com

Luigi Vanfretti
ESCE Department
Rensselaer Polytechnic Institute
Troy, NY, USA

Chetan Mishra, Jaime De La Ree Jr., Kevin D Jones
Dominion Energy, Inc.
Glen Allen, VA, USA

***Abstract*— This paper examines an unusual dynamic phenomenon observed at a wind power plant connected to Dominion Energy's transmission system. The phenomenon is characterized by irregular non-sinusoidal reactive power output without a fixed frequency, which differs from conventional oscillatory responses. Although initially identified as an oscillation by monitoring tools, detailed analysis using synchrophasor data revealed that the anomaly originates from the plant's control logic rather than controller-to-grid interaction dynamics. Specifically, the root cause is the truncation of power factor setpoints to three decimal places when converting reactive power commands from the Power Plant Controller into turbine-level instructions, creating a quantization-like effect that limits the control signal to a discrete set of values. This constraint leads to abrupt reactive power changes during voltage regulation, producing step-like patterns and erratic behavior. The paper presents field observations, explains the mechanism behind this response, and demonstrates its impact through a proof-of-concept illustration focused on explaining the controller observed behavior. These findings highlight the need for improved communication protocols, accurate control modeling, and improved measurement-based validation to prevent control-induced anomalies as inverter-based resources continue to reshape the dynamics of power systems.**

***Index Terms*— Inverter-based resources, power plant controller, power factor, synchrophasors, truncation, wind power plants.**

I. Introduction

THE increasing integration of inverter-based resources (IBRs) such as wind and solar plants is reshaping the dynamic behavior of today's power systems [1]. IBRs introduce control algorithm-dependent behavior leading to new forms of dynamic responses and instabilities that are not well understood or captured by conventional simulation models. Recent literature has highlighted a growing number of field-observed phenomena, including low-frequency oscillations [2], [3]. These events are difficult to reproduce in simulation environments due to the inadequacy of existing IBR models, which when available, fail to include realistic representations of their underlying control algorithms. This is expounded by the fact that for several IBR plants, simulation models may not even exist. Synchrophasors have emerged as a critical resource in this context, enabling high-resolution monitoring and diagnostic capabilities that help bridge the gap between observed behavior [2], [3] and model-based analysis [4], and are indispensable when models are not available.

The paper investigates a newly identified dynamic mechanism observed at a grid-connected wind power plant (WPP), characterized by irregular, non-sinusoidal reactive power behavior with no fixed frequency, exhibiting patterns that deviate significantly from conventional power system dynamics. We will start by presenting the observed behavior at a WPP within Dominion Energy's power system using high-resolution synchrophasor measurements, provide details of the plant under study, explain the initiation mechanism of the instability, and demonstrate the underlying mechanism through simulations on a simplified model.

The observed behavior arises from the set-point communication of the plant-level control system. The Power Plant Controller reactive power set-points generated (PPC) are converted into truncated power factor references, which result in a quantization-like effect that restricts the controller output to a finite set of discrete states, thereby inducing discontinuous reactive power adjustments. While the use of direct reactive power (Q) commands can be adopted in modern power plant controllers (e.g., constant reactive power control mode), PF set-point-based control is still present in many existing plants, particularly older ones or those with specific vendor communication protocols, as in the present case. The issue addressed in this work is not the result of a single poorly configured plant-level controller [2], but instead it highlights a class of potential issues arising from discretization and truncation of control signals sent to individual turbines, which can easily be overlooked. It was very difficult to determine the root cause of this case, and this paper aims to contribute to the power industry's knowledge by raising awareness of this challenging issue. This work builds on prior efforts in measurement-based dynamic analysis [3], [5] and emphasizes the benefit of systematic synchrophasor data analysis and the need for accurate and validated modeling approaches with enhanced measurement data integration.

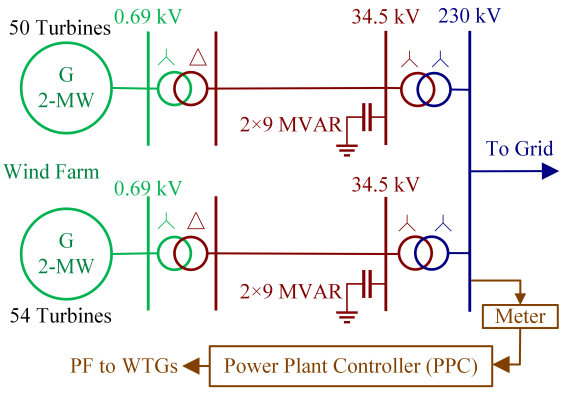

Fig. 1. Simplified diagram of the wind power plant under study.

II. Wind Power Plant Under Study

A simplified diagram of the plant is shown in Fig. 1. The WPP study has an output capacity of 208 MW, consisting of 104 doubly-fed asynchronous wind turbine generators (WTGs), each rated at 2 MW. The WTGs operate at a voltage of 690 V and are connected via 104 step-up transformers (0.69 kV/34.5 kV). The transformers are grouped into two collectors: the first collector has 50 transformers, and the second has 54 transformers, forming two feeders, one for each WT. These feeders are connected to the plant substation. Each of the two 34.5 kV plant substation buses is equipped with two 9 MVAR capacitor banks. The interconnection substation consists of two generation step-up transformers (GSUTs), which connect the feeders to the 34.5 kV/230 kV transmission system, serving as the point of interconnection (POI). The WTGs maintain an almost constant reactive capability of ±680.4 kVar at 1 pu voltage throughout the entire operating range of the turbine. However, when plant power falls below approximately 5%, the reactive capability gradually decreases to 0 MVAR. Additionally, the reactive capacity drops to 0 MVAR when the generator terminal voltage is below 0.9 pu or above 1.1 pu.

III. Event Description

A. First Observation

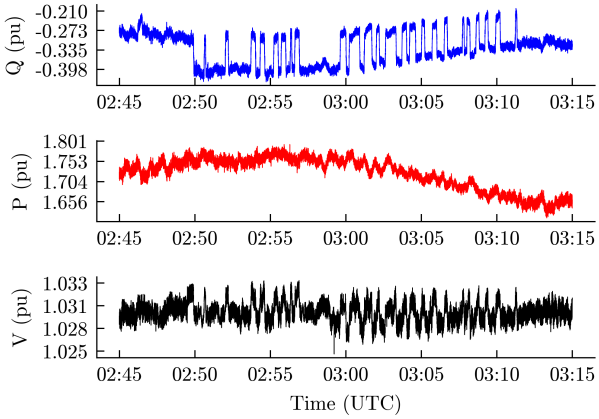

Fig. 2. Reactive power, active power, and voltage plots at the output of the wind power plant during the event on March 13, 2024.

The behavior addressed in this paper was first reported on March 13, 2024, starting at approximately 2:50 AM (UTC). Fig. 2 shows the reactive power (Q), active power (P) and voltage (V) measured at the POI during the event. As evident in Q, it is an abnormal dynamic behavior with irregular and non-sinusoidal dynamics. This dynamic response is only seen by the Q signal, but not by P, which is a behavior caused by the PPC [6].

B. Detection and Operational Impact

The oscillation detection tool in use at Dominion Energy reported this behavior as an oscillation in the frequency range [0.05, 0.15] Hz by raising an alarm. The tool is composed of four RMS-energy-based oscillation detectors running in parallel to analyze distinct frequency bands. For a signal $x(n)$ of length N, the RMS energy is given, as

$$RMS = \sqrt{\frac{1}{N}\sum_{n=0}^{N-1} x^2(n)} \quad (1)$$

where x is the signal being measured and N the total number of points in a sliding window being used to compute the RMS.

The theoretical background of RMS-energy detectors, preprocessing steps, and details of the bandpass filters can be found in [7], [8], [9]. The application monitors multiple signals from PMUs in real-time across various frequency ranges and generates an alarm if pre-configured thresholds are exceeded [10], [11].

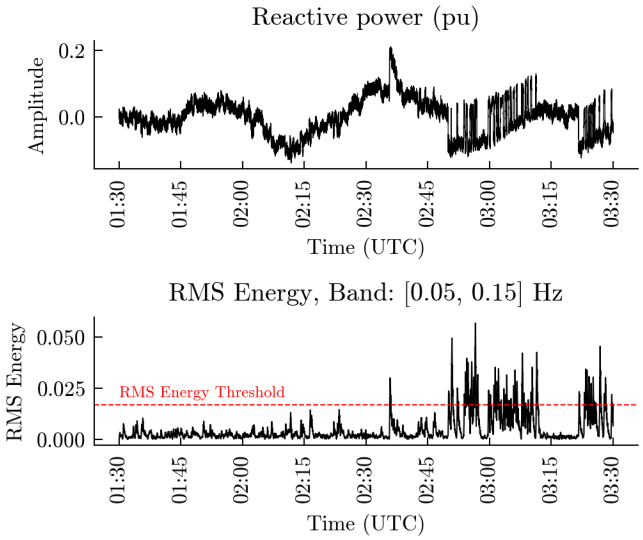

Fig. 3: Reactive power (top) and its RMS-energy (bottom) during ambient conditions (01:30 – 02:50 AM) and during the abnormal behavior which starts after 02:50 AM (UTC).

In Fig. 3, the reactive power of the signal at POI and its corresponding RMS-energy calculated using a 5 second sliding window is shown for the band [0.05, 0.15] Hz, where the event was detected when the RMS-energy crossed a pre-determined threshold. It can be observed that the abnormal behavior shown is not an oscillation and erroneously categorizing it as one can have following operational impacts.

- It may trigger frequent and unnecessary alarms, potentially cause operator fatigue and reduce overall system responsiveness.
- It could result in minor voltage flickers or slight degradation of power quality, impacting equipment performance.
- It carries the risk of unforeseen interactions with other plant control systems, which may lead to other plant performance issues.

Mitigation strategies: We note that the WPP facility owner has already implemented a ±0.5 kV deadband as an initial mitigation measure, and they are currently evaluating further options.

C. Time-Frequency Analysis Using Wavelet Transform

Time-frequency analysis is essential for characterizing non-stationary, aperiodic and non-sinusoidal signals whose spectral content varies with time. Unlike classical Fourier analysis, which provides frequency information averaged over the entire duration of the signal and assumes stationarity, time-frequency methods reveal how frequency components evolve temporally, allowing the detection and precise time-frequency characterization of events [12]. The continuous wavelet transform (CWT) provides such a time-frequency representation by decomposing signal $x(t)$ into wavelet coefficients $W_x(a,b)$, given by,

$$W_x(a,b) = \int_{-\infty}^{\infty} x(t)\psi^*_{a,b}(t)dt \tag{2}$$

where the analyzing wavelet $\psi_{a,b}(t)$ is a scaled and shifted version of a mother wavelet $\psi(t)$ as given by,

$$\psi_{a,b}(t) = \frac{1}{\sqrt{|a|}}\psi\left(\frac{t-b}{a}\right) \tag{3}$$

with the scale parameter a inversely related to the frequency and the translation b localizing the transformation in time [12]. The Morlet wavelet is widely applied due to its optimal joint time-frequency concentration, which is given, by

$$\psi_{Morlet}(t) = \pi^{-\frac{1}{4}}(e^{j\omega_0 t} - e_0^{-\omega_0^2/2})\ e^{-\frac{t^2}{2}} \tag{4}$$

where ω_0 is the central frequency.

The spectrogram is plotted with the time on the horizontal axis and central frequency corresponding to each wavelet scale on the vertical axis. The intensity of the color represents the localized signal energy, $|W_x(a,b)|^2$, enabling clear visualization of how the spectral components evolve over time and frequency.

Figure. 4 shows the spectrogram of the reactive power signal at the output of the plant for a two-hour interval, which is the same window of data analyzed in Fig. 3. The spectrogram reveals that, during the event, the signal's energy is concentrated predominantly in the lower frequency range, with noticeable temporal variation in frequency content. To obtain this time–frequency representation, we employed a CWT using the Morlet wavelet with a dimensionless central frequency parameter of $\omega_0 = 6$. This parameter determines the number of oscillations within the Gaussian envelope, thereby governing the trade-off between time and frequency resolution.

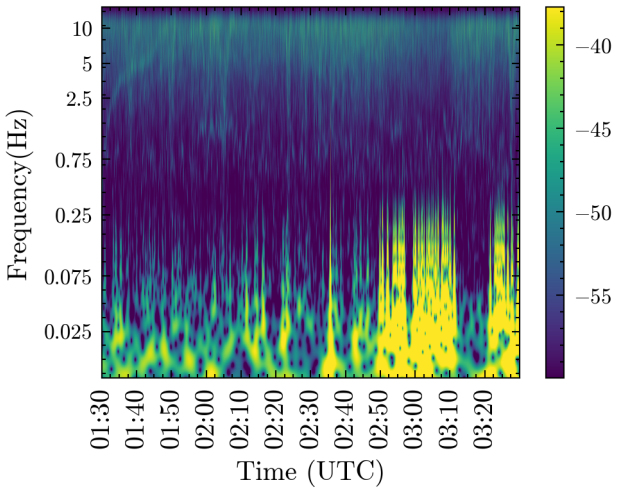

Fig. 4: Spectrogram of the reactive power signal at the output of the wind power plant for two hours starting at 01:30 AM (UTC).

IV. Voltage Regulation In IBR-Based Plants

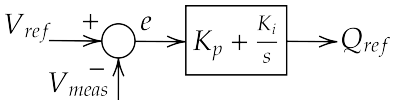

Fig. 5. Voltage control logic at used by the WPP PPC.

IBRs such as WPPs, use PPCs to control voltage at the POI. A common approach is to use a Proportional-Integral (PI) Controller to regulate reactive power output based on voltage deviation, as shown in Fig. 5, which is used in the WPP PPC in Fig. 1. The reactive power reference (set-point signal) is obtained using a PI controller as follows:

$$Q_{ref}(t) = K_p.e(t) + K_i\int_0^t e(\tau)d\tau \tag{5}$$

where $Q_{ref}(t)$ is the reactive power reference, $e(t) = V_{ref} - V_{meas}(t)$ is the voltage error and, K_p and K_i are the proportional and integral gains, respectively. This reference is then distributed to individual inverters according to their reactive power, which adjust their output accordingly.

V. The Underlying Mechanism Giving Rise to Irregular Dynamics at the WPP

The WPP under study regulates the voltage at the POI via a PPC, which employs a PI controller as described in Section IV. The PPC determines the required reactive power (Q_{ref}) based

on the voltage error and transmits this as a command to the inverters. However, at this site, the inverters cannot receive Q_{ref} directly. Instead, the PPC translates the computed Q_{ref} into an equivalent power factor (PF) reference. This conversion introduces a quantization-like effect, which is the root cause of this observed WPP response (see Fig. 2).

The PF setpoint is calculated using the measured P and the Q_{ref} determined by the PPC. However, due to limitations in the communication channel, the PF values sent to the inverters are truncated to three decimal places. While the PPC can compute Q_{ref} with sufficient precision, the control command to the inverters is limited to a discrete set of PF values (three decimals), as shown in Fig. 6.

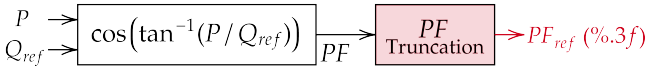

Fig. 6: Q_{ref} from PPC is used to calculate the PF which is truncated to 3 decimals and set as the setpoint to each individual wind turbine.

Furthermore, the site is restricted to operating within a PF of 0.95 to 1. Given the three-decimal place constraint, only a finite number of PF set point values are possible, specifically: 0.950, 0.951, 0.952, …, 0.999, 1.000, as shown on the x-axis of the plots in Fig. 7. This results in discontinuities in the plant's reactive power output whenever a new PF reference is issued. The magnitude of the resulting Q will have discrete changes (see the square-like patterns in Fig. 2) that depend on both the actual active power output and the PF reference in effect.

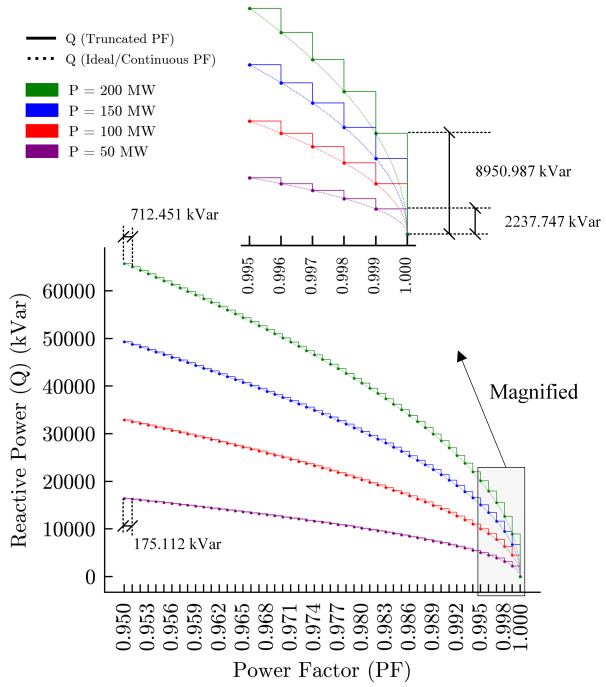

Fig. 7. Reactive power corresponding to various PF references for four different levels of active power output.

Figure. 7 illustrates the Q corresponding to various PF reference values across four distinct levels of P output, each represented by a different color. The discrete points indicate the achievable Q values under the site's communication constraints, reflecting the realizable PF commands. The solid curves highlight the stepwise or discontinuous transition in Q, a result of the limited and discrete set of PF values.

Focusing on the zoomed region, representing high PF conditions, consider a scenario where the WPP operates at 200 MW with a PF of 1.000. A slight voltage drop at the POI prompts the PPC to issue a Q_{ref} to correct this deviation. However, the next available PF value below 1.000 is 0.999, which corresponds to a reactive power injection of 8950.987 kVar, more than necessary to restore the voltage. In the subsequent control cycle, the overcorrection results in a voltage overshoot, prompting the PPC to revert the PF command back to 1.000. This back-and-forth, results in the behavior shown in Fig. 2.

The severity of the deviations in Q is strongly influenced by the plant's actual P output. For instance, under the same PF transition from 1.000 to 0.999, but at 50 MW, the corresponding jump in reactive power is only 2,237.747 kVar, substantially smaller. This indicates that the observed WPP response is most pronounced during high active power operation. In practice, at Dominion Energy, the oscillation detection tool frequently flags such behavior during periods of elevated MW output. Explanations on why this kind of signal perceived as an oscillation by the tool can be found in [3].

At lower power factors (see the left side of Fig. 7), although the truncated PF steps can introduce Q discontinuities, the changes are smaller in absolute terms. For example, transitioning from 0.950 to 0.951 PF results in a jump of 712.451 kVar at 200 MW, and just 175.112 kVar at 50 MW. Although these discontinuities are less severe, the Q required to maintain voltage regulation is generally larger at lower PFs. Consequently, this plant typically operates at PF close to unity to minimize the reactive power burden.

VI. Proof-of-Concept Simulation Illustrating The PF Truncation Mechanism

In this section, we present a proof-of-concept simulation that illustrates the mechanism discussed earlier. Specifically, we show how truncating the PF to three decimal places can lead to irregular, non-sinusoidal reactive power output, similar to what was observed in actual measurements. The illustration is not intended to replicate the response of the real WPP analyzed in the previous sections, as doing so would require detailed models of both the wind farm and the rest of the grid, which do not exist. Instead, the objective is to capture the essence of the mechanism and its impact using a simplified model. The focus of this illustration is exclusively on the plant-level controller behavior and to demonstrate the direct link between truncated PF and resulting Q behavior. Since the phenomenon is at the

controller logic level, not a dynamic interaction between the grid and the WPP, we chose a simple model to show the cause-and-effect relationship without adding complexity that might obscure the illustration. The illustration was implemented using the Python Control Systems Library.

Figure. 8 shows a simplified PI-type voltage control that mimics the setup at the plant under study. The controller (*C* in Fig. 8) outputs a Q_{ref} command based on voltage error using V_{ref} (the reference voltage) and V_m (the measured voltage), which is then converted to a PF value. This PF is truncated to three digits after the decimal, resulting in PF_{ref}, and sent to the inverters. The inverters are assumed to be fast and stable operating under this PF and the *P* output. Note that *d* represents changes in the grid, such as variations in the load under ambient conditions, and H_v is the voltage sensor model.

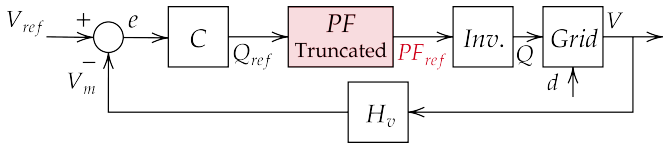

Fig. 8. Block diagram of the model for the illustration of the PF truncation mechanism.

To represent the slow plant dynamics, the voltage response of the grid is modeled as a static function of Q, using the relation $V = a_0 + a_1 Q$. The values of PI controller parameters are set to $K_P = 1$ and $K_I = 0.25$, with a voltage reference of $V_{ref} = 1$ pu.

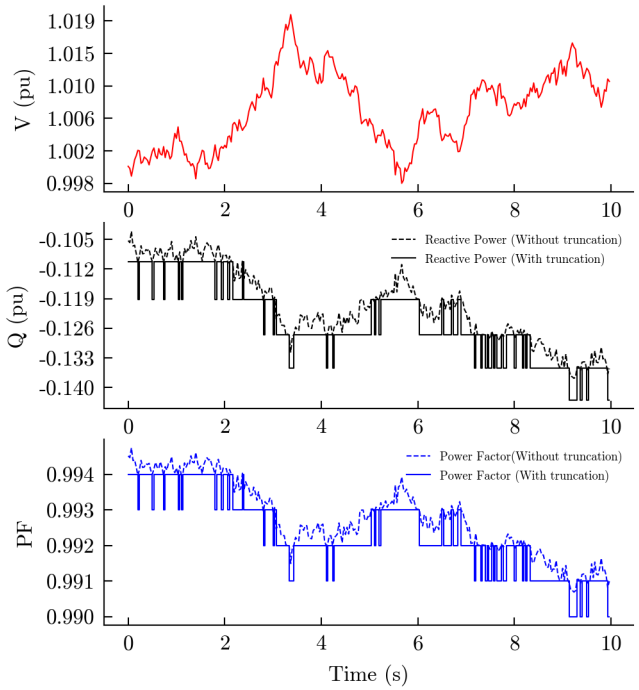

Fig. 9. Voltage, reactive power, and power factor plots generated for the illustration of the PF truncation mechanism. Reactive power and power factor plots show simulation result with and without truncation mechanism.

As shown in Fig. 9, a small voltage deviation leads to abnormal Q behavior when PF is limited to three decimal places. In addition, Fig. 9 also shows a plot of the PF signal with and without truncation. When truncated to three decimals, the PF jumps between discrete values, which introduces step-like changes in Q. This results in the kind of erratic reactive power dynamics that we aim to highlight in this illustration. The primary objective is to demonstrate the underlying principle of PF truncation, focusing on its conceptual framework and operational logic, rather than trying to replicate actual field conditions.

VII. Conclusion

This study provides a detailed analysis of an abnormal dynamic response observed at a grid-connected wind power plant, using real-world synchrophasor data. The investigation reveals that the phenomenon is not an oscillation steaming from conventional system dynamics, but a power plant controller-induced mechanism rooted in the truncation of power factor setpoints within the plant-level controller communications. By converting Q commands into PF references and limiting them to three decimal places, the PPC introduces a quantization effect that restricts control signals to discrete increments, resulting in abrupt reactive power transitions and irregular voltage regulation.

The proof-of-concept simulations validate this mechanism conceptually, demonstrating how truncation alone can produce the observed non-sinusoidal aperiodic behavior such as the one observed in the WPP in Dominion Energy's power system. It is important to note that the underlying mechanism could be illustrated using a simplified simulation model. The lack of adequate simulation models for this plant makes it futile to attempt to recreate the event through detailed simulation models, illustrating that modeling adequacy is not a matter of using highly granular models, but to have models available that are able to represent real-world dynamic performance.

These findings highlight critical gaps in current modeling practices for inverter-based resources and emphasize the importance of integrating high-resolution field measurements into dynamic studies. As the penetration of IBRs continues to grow, addressing such PPC-induced behaviors through improved communication protocols, enhanced control system design, and measurement-based validation will be essential for maintaining system stability and operational reliability.

References

[1] B. Kroposki *et al.*, "Achieving a 100% Renewable Grid: Operating Electric Power Systems with Extremely High Levels of Variable Renewable Energy," *IEEE Power Energy Mag.*, vol. 15, no. 2, pp. 61–73, Mar. 2017, doi: 10.1109/MPE.2016.2637122.

[2] C. Mishra, L. Vanfretti, J. Delaree, and K. D. Jones, "Analyzing a Non-Sinusoidal Response from a Real-World Solar PV," *IEEE Trans. Power Syst.*, vol. 39, no. 2, pp. 4771–4774, Mar. 2024, doi: 10.1109/TPWRS.2024.33

[3] B. Pudasaini, L. Vanfretti, C. Mishra, J. De La Ree and K. D. Jones, "Dynamic Performance Analysis of an Inverter-Based PV Plant during

Sunrises and Sunsets through Synchrophasors," 2025 IEEE Power & Energy Society General Meeting (PESGM), Austin, TX, USA, 2025, pp. 1-5, doi: 10.1109/PESGM52009.2025.11225625.

[4] O. Saad, H. Honvo, A. Ajaja, S. Dennetière, and Y. Vernay, "Battery energy storage system integration to the RTE network: from EMT studies to site validation," in *22nd Wind and Solar Integration Workshop (WIW 2023)*, Sept. 2023, pp. 198–204. doi: 10.1049/icp.2023.2738.

[5] C. Mishra, L. Vanfretti, J. Delaree, T. J. Purcell, and K. D. Jones, "Understanding the inception of 14.7 Hz oscillations emerging from a data center," *Sustain. Energy Grids Netw.*, vol. 43, p. 101735, Sept. 2025, doi: 10.1016/j.segan.2025.101735.

[6] D. Pattabiraman and P. Bixel, "Minimizing Interactions Between Power Plant Controller and Inverters in IBR Plants," in *2024 IEEE/PES Transmission and Distribution Conference and Exposition (T&D)*, May 2024, pp. 1–5. doi: 10.1109/TD47997.2024.10555959.

[7] J. F. Hauer and F. Vakili, "An oscillation detector used in the BPA power system disturbance monitor," *IEEE Trans. Power Syst.*, vol. 5, no. 1, pp. 74–79, Feb. 1990, doi: 10.1109/59.49089.

[8] L. Vanfretti, M. Baudette, J.-L. Domínguez-García, M. S. Almas, A. White, and J. O. Gjerde, "A PMU-based fast real-time oscillation detection application for monitoring wind farm-to-grid sub-synchronous dynamics," *Electric Power Components and Systems*, 2012.

[9] J. Follum, J. Holzer, and P. Etingov, "A statistics-based threshold for the RMS-energy oscillation detector," *Int. J. Electr. Power Energy Syst.*, vol. 128, p. 106685, June 2021, doi: 10.1016/j.ijepes.2020.106685.

[10] T. J. Purcell, "Case Study: Enhancing Grid Reliability in the Presence of Inverter-Based Resources Through Advanced Oscillation Detection and Mitigation," presented at the 51st Annual Western Protective Relay Conference, Spokane, Washington, Oct. 2024. [Online]. Available: ttps://selinc.com/api/download/140372/

[11] T. J. Purcell, J. Wold, M. A. Kahn, and J. Bestebreur, "Inverter-Based Resource (IBR), Oscillations, and Grid Reliability," PAC World. Accessed: Oct. 29, 2025. [Online]. Available: https://www.pacw.org/inverter-based-resource-ibr-oscillations-and-grid-reliability

[12] C. Mishra, L. Vanfretti, J. De La Ree, and K. D. Jones, "Automatically Discerning Power System Dynamics in Synchrophasor Measurements Data Spectra," in *2023 IEEE Power & Energy Society General Meeting (PESGM)*, July 2023, pp. 1–5. doi: 10.1109/PESGM52003.2023.10252802.